

Experimental and Theoretical Study of the OH-Initiated Degradation of Piperazine under Simulated Atmospheric Conditions

Wen Tan, Liang Zhu,[#] Tomas Mikoviny, Claus J. Nielsen,* Armin Wisthaler, Barbara D'Anna, Simen Antonsen, Yngve Stenström, Naomi J. Farren, Jacqueline F. Hamilton, Graham A. Boustead, Alexander D. Brennan, Trevor Ingham, and Dwayne E. Heard

Cite This: <https://dx.doi.org/10.1021/acs.jpca.0c10223>

Read Online

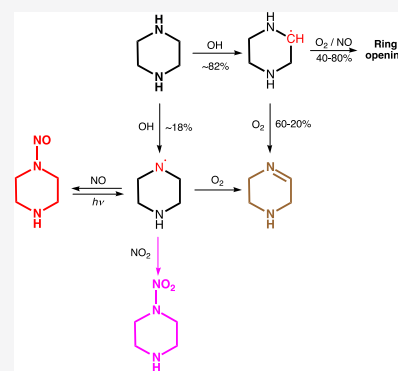
ACCESS |

Metrics & More

Article Recommendations

Supporting Information

ABSTRACT: The OH-initiated photo-oxidation of piperazine and 1-nitropiperazine as well as the photolysis of 1-nitrosopiperazine were investigated in a large atmospheric simulation chamber. The rate coefficient for the reaction of piperazine with OH radicals was determined by the relative rate method to be $k_{\text{OH-piperazine}} = (2.8 \pm 0.6) \times 10^{-10} \text{ cm}^3 \text{ molecule}^{-1} \text{ s}^{-1}$ at $307 \pm 2 \text{ K}$ and $1014 \pm 2 \text{ hPa}$. Product studies showed the piperazine + OH reaction to proceed both via C–H and N–H abstraction, resulting in the formation of 1,2,3,6-tetrahydropyrazine as the major product and in 1-nitropiperazine and 1-nitrosopiperazine as minor products. The branching in the piperazinyl radical reactions with NO, NO₂, and O₂ was obtained from 1-nitrosopiperazine photolysis experiments and employed analyses of the 1-nitropiperazine and 1-nitrosopiperazine temporal profiles observed during piperazine photo-oxidation. The derived initial branching between N–H and C–H abstraction by OH radicals, $k_{\text{N-H}}/(k_{\text{N-H}} + k_{\text{C-H}})$, was 0.18 ± 0.04 . All experiments were accompanied by substantial aerosol formation that was initiated by the reaction of piperazine with nitric acid. Both primary and secondary photo-oxidation products including 1-nitropiperazine and 1,4-dinitropiperazine were detected in the aerosol particles formed. Corroborating atmospheric photo-oxidation schemes for piperazine and 1-nitropiperazine were derived from M06-2X/aug-cc-pVTZ quantum chemistry calculations and master equation modeling of the pivotal reaction steps. The atmospheric chemistry of piperazine is 23 evaluated, and a validated chemical mechanism for implementation in dispersion models is presented.



1. INTRODUCTION

Piperazine (1,4-diazacyclohexane, PZ) is among the amines considered for use in large-scale Carbon Capture (CC) to reduce CO₂ emissions from industrial point sources.¹ A 40 wt % amine solution with PZ and 2-amino-2-methyl-1-propanol in a 1:2 M ratio was recently suggested as the new benchmark solvent for CO₂ capture technology.² Measurements at the Technology Centre Mongstad (TCM; Norway) have established that at times it can be difficult to avoid ppm-level emissions of amines and their process degradation products to the environment during operation of a large-scale capture plant³—the concern being that carcinogenic nitrosamines and nitramines are either directly emitted or formed in the subsequent atmospheric photo-oxidation of the fugitive amines.⁴ The Norwegian Institute for Public Health recommends that the total amount of nitrosamines and nitramines in the atmosphere should be below 0.3 ng m⁻³ in air and below 40 ng dm³ in drinking water for a risk level of 10⁻⁵.⁴ Such low detection levels are currently virtually impossible to monitor with today's technology, and it is consequently imperative to acquire quantitative information on the degradation pathways for the relevant amines under

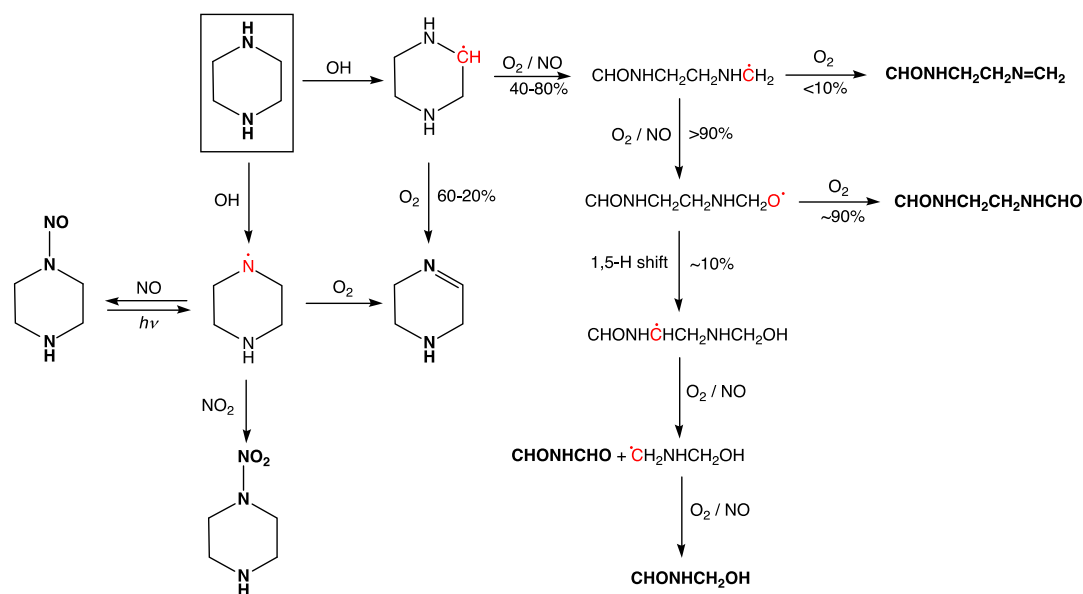
atmospheric conditions and to implement this information in reliable chemical models for dispersion calculations.

The major removal processes of gaseous PZ in the atmosphere are uptake in aqueous particles and gas phase reaction with OH radicals during daytime and NO₃ radicals during nighttime. The OH radical reaction with PZ was recently reported to be very fast, $\sim 2.3 \times 10^{-10} \text{ cm}^3 \text{ molecule}^{-1} \text{ s}^{-1}$ at 298 K and to favor C–H abstraction: $k_{\text{N-H}}/(k_{\text{N-H}} + k_{\text{C-H}}) = 0.09 \pm 0.06$.⁵

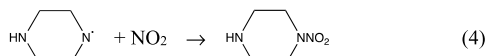
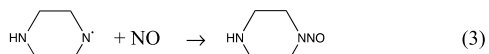
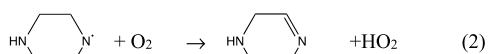
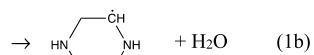
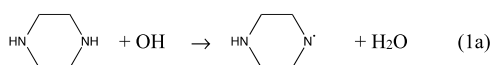
The PZ nitrosamine (1-nitrosopiperazine, PZNO) and nitramine (1-nitropiperazine, PZNO₂) are both carcinogenic;⁴ they result from the following sequence of atmospheric gas-phase reactions⁶

Received: November 12, 2020

Revised: December 16, 2020

Scheme 1. Quantum Chemistry Prediction of the Major Primary Products in the OH-Initiated Atmospheric Photo-Oxidation of Piperazine (PZ)^a

^aRadical sites are indicated with red, thermally stable molecules are shown in boldface.



Although the O₂ reaction with aminyl radicals, R₁R₂N•, is reported to be around 6 orders of magnitude slower than the corresponding NO and NO₂ reactions,⁷ it is still dominating under most atmospheric conditions, and PZNO and PZNO₂ are thus only expected as minor products in the natural atmospheric photo-oxidation of PZ. Both compounds were observed, but not quantified, in previous PZ photo-oxidation experiments in the ~200 m³ European Photoreactor (EUPHORE),⁸ and in the more recent experiments employing a ~18 m³ indoor smog chamber.⁹

The open literature includes two theoretical studies on the kinetics of the hydrogen abstraction from PZ by OH radicals, in which the branching between the N–H and C–H abstraction reactions 1a and 1b were predicted to be 0.07¹⁰ and 0.01,¹¹ respectively, at 298 K. The latter theoretical study also includes an investigation of the atmospheric degradation following the C–H abstraction. A theoretical report of the Cl-atom-initiated oxidation of PZ suggests that this reaction proceeds with 99.8% N–H abstraction at 298 K;¹² the study also includes a mapping of the potential energy surfaces for the piperazinyl radical reactions with NO and O₂.

In the present communication, we report results from a series of PZ and PZNO₂ photo-oxidation and PZNO photolysis experiments in the EUPHORE chamber, and quantum chemistry-based evaluations of the major routes in

the OH initiated photo-oxidations of PZ and PZNO₂ under atmospheric conditions. The new results pave the way for the first reliable environmental impact assessments of realizing large-scale CC-facilities based on PZ-containing solvents.

2. METHODS

2.1. Experimental Methods and Chemicals. A series of 87 experiments was carried out in chamber B of the EUPHORE 88 facility in Valencia, Spain. The facility and analytical methods 89 have recently been reported in detail¹³—special on-line 90 instrumentation include a PTR-TOF 8000 instrument 91 (IONICON Analytik GmbH, Innsbruck, Austria), a prototype 92 CHARON inlet^{14,15} interfaced to a second PTR-TOF 8000, a 93 compact time-of-flight Aerosol Mass Spectrometer (C-ToF- 94 AMS, Aerodyne Research Inc., Billerica, MA, U.S.A.),¹⁶ and a 95 FAGE (Fluorescence Assay by Gas Expansion) apparatus.¹⁷ 96 Additional information specific to the present work is given in 97 the Supporting Information. 98

Information on chemicals used and the synthesis of PZNO 99 and PZNO₂ is found in the Supporting Information. 100

2.2. Computational Methods. Optimized geometries of 101 stationary points on the potential energy surfaces for the 102 atmospheric degradation of PZ were obtained in M06-2X¹⁸ 103 calculations employing the aug-cc-pVTZ^{19,20} basis set. Pre- and 104 postreaction complexes were located by following the intrinsic 105 reaction coordinate^{21–24} from the saddle points. Electronic 106 energies of selected stationary points were improved by 107 explicitly correlated coupled cluster calculations with scaled 108 triples contributions, denoted CCSD(T*)-F12a.^{25,26} Reaction 109 enthalpies and proton affinities were calculated using the G4 110 model chemistry.²⁷ Dipole moments and isotropic polar- 111 izabilities, serving as input to prediction of ion-molecule 112 reaction rate coefficients,²⁸ were obtained in M062X/aug-cc- 113 pVTZ and B3LYP/aug-cc-pVTZ calculations; see Table S1 in 114 the Supporting Information. The M06-2X, B3LYP, and G4 115 calculations were performed in Gaussian 09;²⁹ the CCSD(T*)- 116 F12a calculations were carried out employing Molpro 117 2012.1.^{30,31} 118

Master equation calculations were carried out using the program MESMER 3.0³² (Master Equation Solver for Multi-Energy-Well Reactions) to simulate the reactions under atmospheric conditions. The required input parameters for molecules, intermediate species, and products were obtained from the ab initio calculations.

3. RESULTS

3.1. Computational Results. The kinetics of the initial step in the PZ + OH reaction is complicated by PZ existing in three low-energy chair conformations (*eq-eq*, *eq-ax*, and *ax-ax*) with relative enthalpies of 0, 2.44, and 6.92 kJ mol⁻¹, respectively (values from G4 calculations). Consequently, the conformational equilibrium will consist of around 55% *eq-eq*, 42% *eq-ax*, and 3% *ax-ax* at 298 K. This issue was not considered in the previous theoretical studies of the reaction, and a detailed theoretical account of the kinetics and of the branching between C–H and N–H abstraction in the initial step is far from trivial and considered outside the scope of the present work.

The theoretical prediction of the major routes in the atmospheric degradation of PZ is summarized in Scheme 1. The degradation routes largely concord with those established in previous dimethylamine^{7,33,34} and diethylamine^{8,33} photo-oxidation experiments. Details of the quantum chemistry study are collected in the Supporting Information, including illustrations of the pivotal potential energy surfaces, Figures S1–S5, and the associated Tables S2–S6 containing energies, Cartesian coordinates, and vibration-rotation data employed in master equation calculations.

The present mechanistic assessment differs notably from that recently offered based on G4 calculations.¹¹ First, our study includes a mapping of the atmospheric PZ aminyl radical reactions under atmospheric conditions suggesting a slightly different, and simpler scheme than that first suggested and applied by Lindley et al.⁷ in their analysis of the (CH₃)₂N radical reactions with O₂, NO and NO₂. The difference being that the piperazinyl + NO₂ reaction leading to the corresponding imine is blocked by a barrier of around 12 kJ mol⁻¹ above the entrance energy of the reactants. Another result from the present theoretical study is that the barrier to reaction 2 is calculated to be ~10 kJ mol⁻¹ higher than in the corresponding (CH₃)₂N + O₂ reaction, indicating that PZ has a higher potential to nitrosamine and nitramine formation than dimethylamine per aminyl radical.

Second, we find the cyclic alkoxy radical, that ultimately follows C–H abstraction, to be metastable resulting in spontaneous ring opening, and that the major fraction of the resulting CHONHCH₂CH₂NHCH₂ radical will end up as a diamide. The calculated branching between ring-opening and formation of the PZ imine, 1,2,3,6-tetrahydropyrazine (PZI), is very sensitive to the barrier height and cannot be accurately predicted from theoretical calculations. In summary, the present theoretical study predicts that under ambient conditions with NO > 2 ppb, the major products following C–H abstraction from PZ will be 60–20% PZI, 32–65% CHONHCH₂CH₂NHCHO, 4–8% CHONHCH₂CH₂N=CH₂, and 4–7% CHONHCHO and CHONHCH₂OH.

Third, we have also assessed the atmospheric fate of PZNO₂—one of the carcinogenic PZ photo-oxidation products. The major photo-oxidation routes for PZNO₂, outlined in Scheme S1 in the Supporting Information, parallel to those of PZ with one exception—the alkyl-radical formed

upon ring-opening ejects NO₂ resulting in the same amide/imine that was also predicted as a primary product in the PZ + OH reaction. Details of the quantum chemistry study of the OH radical-initiated atmospheric PZNO₂ photo-oxidation are found in the Supporting Information (including Figure S6 illustrating the potential energy surface to ring-opening and subsequent NO₂-ejection, and the underlying quantum chemistry data in Table S7).

Previous photo-oxidation studies of PZ have demonstrated not only experimental challenges but also disagreement in the understanding of the underlying mechanism.^{8,9} The present theoretical study offers a detailed mechanistic insight and an accurate prediction of the product distribution, facilitating a comprehensive interpretation of the experimental photo-oxidation experiments which are described below.

3.2. Experimental Results. We first report results from kinetic studies of the PZ + OH reaction. We then present results from PZNO₂ photo-oxidation experiments and from PZNO photolysis experiments facilitating interpretation of the *pièce de résistance*—the atmospheric PZ photo-oxidation. Finally, we present results from studies of the aerosol formed in the PZ photo-oxidation experiments.

3.2.1. Piperazine + OH Reaction Kinetics. Two relative rate experiments were carried out in the EUPHORE chamber B in which isoprene, limonene, 1,3,5-trimethylbenzene, and pyrrole were used as reference compounds. Acetonitrile was added as an inert tracer to monitor the apparent dilution by purified air that is constantly added to compensate for leakage and continuous sampling by the air monitors ($k_{\text{OH}+\text{CH}_3\text{CN}} = 2.2 \times 10^{-14}$ cm³ molecule⁻¹ s⁻¹ at 298 K).³⁵ OH radicals were generated employing IPN as the precursor: CH₃CH(ONO)-CH₃ h((CH₃CH(O)CH₃ + NO; CH₃CH(O)CH₃ + O₂ → CH₃C(O)CH₃ + HO₂; HO₂ + NO → OH + NO₂).

Figure 1a displays the time evolution of compound-specific PTR–ToF–MS ion signals measured during the second experiment (the first experiment is documented in Figure S7, Supporting Information). The dilution rate because of air replenishment was 8.6×10^{-6} s⁻¹ in the two experiments; PZ wall loss rates (derived from the reagent decay prior to adding IPN) ranged from 1 to 4×10^{-5} s⁻¹. Initial mixing ratios were ~100 ppb for the reference compounds and ~200 ppb for PZ. Average OH densities in the EUPHORE chamber during the periods selected for analyses (9:10–9:30 and 14:10–14:35 UTC) were around 3×10^6 cm⁻³; average pressure and temperature in the two experiments were 1014 ± 2 mbar and 307 ± 2 K. The temporal profile of PZ recorded by the PTR–ToF–MS matches well the one obtained by a home-built high-temperature PTR–MS, indicating an adequate instrument response time for “sticky” substances such as PZ (Figure S8 in the Supporting Information).

A least-squares fitting of the wall- and dilution loss-corrected data (Figure S9 in the Supporting Information) results in an average $k_{\text{OH}+\text{PZ}} = (3.0 \pm 0.6) \times 10^{-10}$ cm³ molecule⁻¹ s⁻¹ at 307 ± 2 K and 1014 ± 2 hPa. Considerable amounts of PZ are, however, transferred from the gas to the particle phase during the periods selected for analysis. Figures S10, S11 (Supporting Information) show the time evolution of aerosol mass and the aerosol PZ content during the kinetic experiments; approximately 6.3 and 1.2% of PZ were lost to the aerosol particles during the two kinetic experiments. Correction for PZ loss to particles during the kinetic experiments was therefore implemented in the data analysis 241

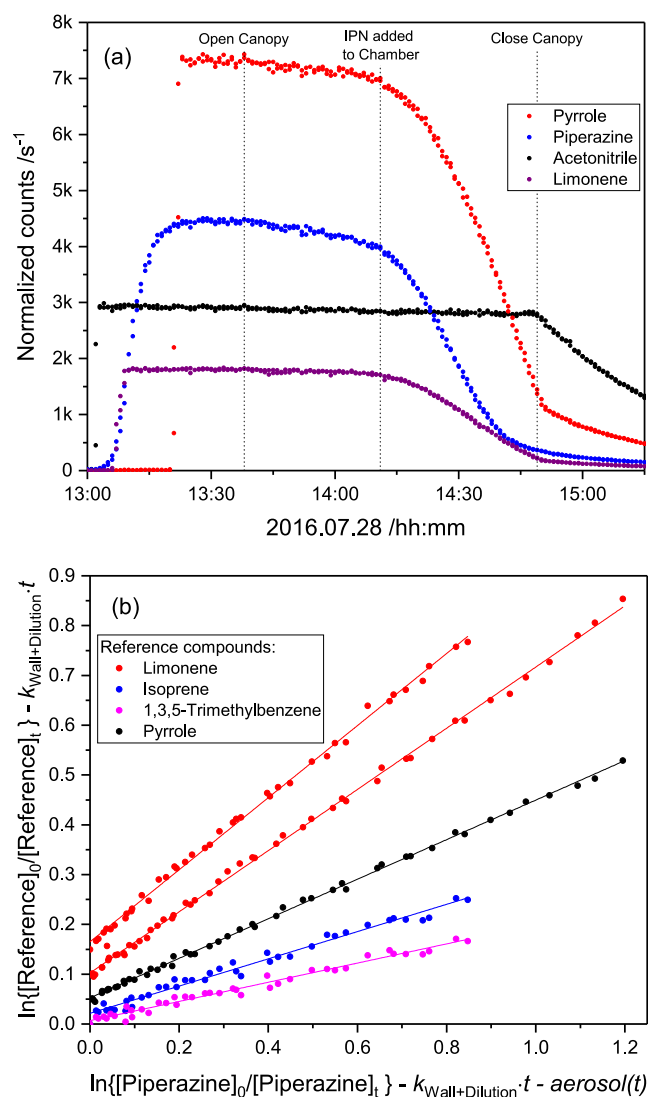


Figure 1. (a): Time evolution of the acetonitrile, pyrrole, PZ and limonene ion signals at m/z 42.034, 68.050, 87.092, and 137.133, respectively, during the second kinetic experiment on 2016.07.28. (b): Relative rate plot showing the decays of isoprene, limonene, pyrrole, and piperazine at 1014 hPa and 307 K in the presence OH radicals. For the sake of clarity, the data have been displaced along the abscissa. The data have been corrected for dilution because of chamber air replenishment, for wall loss and for loss to the aerosol; see Supporting Information.

242 (see Supporting Information for details), resulting in an
 243 average $k_{\text{OH+PZ}} = (2.8 \pm 0.6) \times 10^{-10} \text{ cm}^3 \text{ molecule}^{-1} \text{ s}^{-1}$ at
 244 $307 \pm 2 \text{ K}$ and $1014 \pm 2 \text{ hPa}$, Figure 1b. The present result
 245 agrees well with those of Onel et al.,⁵ who reported $k(T) =$
 246 $(2.37 \pm 0.03) \times 10^{-10} (T/298)^{-(1.76 \pm 0.08)}$ and $k_{\text{OH+PZ}} = (2.25$
 247 $\pm 0.28) \times 10^{-10} \text{ cm}^3 \text{ molecule}^{-1} \text{ s}^{-1}$ at 307 K from flash
 248 photolysis/resonance fluorescence experiments.

249 **3.2.2. 1-Nitropiperazine Photo-Oxidation Studies.** The
 250 atmospheric fate of PZNO₂ was investigated in two photo-
 251 oxidation experiments under high NO and high NO₂ starting
 252 conditions, respectively. This parent compound as well as its
 253 degradation products are very “sticky” and transfer relatively
 254 fast to the chamber walls. In addition, the PZNO₂ photo-
 255 oxidation experiments were accompanied by strong particle
 256 formation with ~50% of the initial PZNO₂ mass being

transferred to particles (see Figure S12 in the Supporting
 Information). This makes quantitative conclusions impossible.
 Figure 2 shows time profiles of the selected mass peaks
 observed during the high-NO photo-oxidation experiment. It is

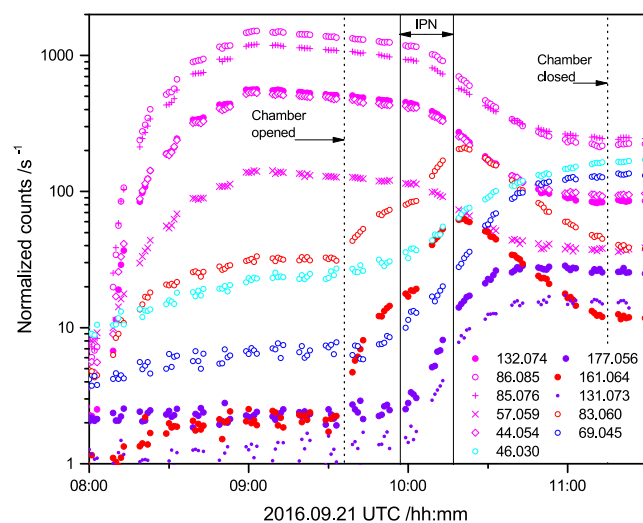


Figure 2. Time profiles of selected ion signals detected during the 1-nitropiperazine (PZNO₂) photo-oxidation experiment on 2016.09.21. Drift tube electric field $E/N = 105 \text{ Td}$.

worth noting that protonated PZNO₂ fragments severely at the
 PTR-ToF-MS instrumental settings employed ($E/N = 105$
 Td): 15% m/z 132.077 (protonated molecule), 38% m/z
 86.084 (NO₂ ejection), 30% m/z 85.076 (HONO ejection),
 4% m/z 57.057 (C₃H₇N⁺, ring fragment), and 13% m/z
 44.050 (C₂H₆N⁺, ring fragment). At $E/N = 65 \text{ Td}$, the fragmentation
 is less pronounced: 44% m/z 132.077, 48% m/z 86.084, 8% m/z
 85.077, <1% m/z 57.057, and <1% m/z 44.050. Consistent
 concentrations of PZNO₂ were derived from both E/N
 settings. The mass peaks related to PZNO₂ photo-oxidation
 are summarized in Table S8 in the Supporting Information.

Figure 2 also demonstrates that PZNO₂ is quite reactive.
 Kinetic data for the CH₃NHNO₂³⁶ and (CH₂)₂NNO₂^{36,37}
 reaction with OH show an order of magnitude reduction in
 reactivity vis-à-vis the parent amines.³⁸ Apparently, the
 deactivating reactivity effect of the electron withdrawing
 nitro group does not extend beyond the adjacent methylene
 groups in PZNO₂.

The 1-nitroso-4-nitropiperazine ([PZ(NO)NO₂]⁺, m/z
 161.067) signal appears the very moment the chamber canopy
 is opened, and it is highly significant that this is paralleled by
 the m/z 83.060 peak. Upon injection of IPN, the increase in
 the m/z 177.062 ion signal, which is unique to 1,4-
 dinitropiperazine [PZ(NO₂)₂], is particularly illustrative.
 In line with the extensive fragmentation of protonated PZNO₂,
 most of the other ion signals observed during the two photo-
 oxidation experiments correspond to molecular fragments,
 Table S8. The m/z 46.029 (CH₄NO⁺) and 69.045 (C₃H₅N₂⁺)
 signals grow throughout the experiments. The former could
 originate from formamide, the latter from imidazole. There are
 no obvious gas phase photo-oxidation routes leading from
 PZNO₂ to these compounds or to their isomers, and we
 tentatively attribute their formation to heterogeneous chem-
 istry; see later.

It is somewhat surprising that the expected major product
 following C–H abstraction—the imine, 1-nitro-1,2,3,6-tetra-

297 hydropyrazine (PZINO₂)—is not revealed by even a trace of
 298 the protonated molecule at *m/z* 130.061. Assuming a similar
 299 fragmentation of protonated PZINO₂ as observed for
 300 protonated PZNO₂, fragment ions are expected at *m/z*
 301 84.068 (NO₂ ejection), 83.060 (HONO ejection), 55.042
 302 (CH₂CH₂N=CH⁺, ring fragment), and 42.034 (CH₂CH₂N⁺,
 303 ring fragment). There is no ion signal detected at *m/z* 84.068,
 304 but the *m/z* 83.060, 55.042, and 42.034 ion signals are all
 305 observed having the expected time profile, Figure 2. Although
 306 the experimental data are not unambiguously conclusive, we
 307 hypothesize that these mass peaks are more than just indicative
 308 of the imine being formed in the PZNO₂ photo-oxidation.

309 **3.2.3. 1-Nitrosopiperazine Photolysis Studies.** Nitros-
 310 amines have a characteristic *n* → *π** transition in the UV-A
 311 region and photolyze rapidly in natural sunlight; the quantum
 312 yield to photo-dissociation of (CH₃)₂NNO following S₀ →
 313 S₁(*nπ**) excitation at 363.5 nm was reported to be 1.03 ±
 314 0.10,³⁹ and theory shows that the excited S₁ state is repulsive
 315 leading to swift dissociation following excitation.⁴⁰ In the
 316 present case, the two primary products expected following
 317 PZNO photolysis are PZI and PZNO₂, Scheme 1.

318 Three photolysis experiments were carried out in the
 319 EUPHORE chamber B. Cyclohexane was added to the
 320 chamber (~2 ppm) for deriving the amount of OH radicals
 321 formed following PZNO photolysis: PZNO h((PZ* + NO;
 322 PZ* + O₂ → PZI + HO₂; HO₂ + NO → OH + NO₂). The
 323 derived OH radical mixing ratio varied between 1 and 4 × 10⁵
 324 cm⁻³ (for details, see Figures S13–S15 and accompanying text
 325 in the Supporting Information).

326 Figure 3 illustrates the ion signal time profiles observed
 327 during the experiments. The mass peaks pertinent to the
 328 PZNO photolysis experiments are summarized in Table 1; a
 329 more complete list of ion signals observed in the experiments is
 330 found in Table S9 in the Supporting Information, which also
 331 includes data from our previous study in which we employed a
 332 PZNO sample of different origin.⁸ It can be seen from Figure 3
 333 that the mass peaks growing in upon photolysis fall in three
 334 categories: (1) the *m/z* 116.082 and 85.076 that decrease in
 335 intensity when the chamber is opened to sunlight, (2) the *m/z*
 336 132.077, 86.084, 83.060, and 44.050 having time profiles
 337 typical of primary photolysis products, and (3) the less intense
 338 *m/z* 97.040, 81.045, 74.024 and 46.029 with time profiles more
 339 resembling those of “secondary” products resulting from
 340 PZNO, PZNO₂, and PZI reactions with OH radicals.

341 An inspection of the ion signals observed in the time period
 342 before opening the chamber canopy (Figure 3) reveals that
 343 also [PZNO]H⁺ fragments at the instrumental settings
 344 employed (*E/N* = 65 Td): 78.5% *m/z* 116.082 (protonated
 345 molecule), 9.8% *m/z* 86.084 (NO ejection), 9.5% *m/z* 85.076
 346 (HNO ejection), and 2.2% *m/z* 44.050 (C₂H₆N⁺ ring
 347 fragment). At *E/N* = 105 Td, the fragmentation is more
 348 severe: 62.8% *m/z* 116.082, 12.6% *m/z* 86.084, 19.8% *m/z*
 349 85.076, and 4.8% *m/z* 44.050. Consistent concentration of
 350 PZNO was derived using both *E/N* settings.

351 Figure 3 further reveals that the expected ion signal of
 352 protonated PZI at *m/z* 85.076 (C₄H₉N₂⁺), to which fragments
 353 of both protonated PZNO and PZNO₂ contribute, apparently
 354 shows more resemblance to that of PZNO than to that of a
 355 primary product like PZI or PZNO₂.

356 The fragmentation of protonated PZNO and PZNO₂
 357 complicates an unambiguous identification of PZI from the
 358 PTR–TOF–MS data: the ion signals at *m/z* 44.050, 85.076,
 359 and 86.084 all originate in both PZNO and PZNO₂. Assuming

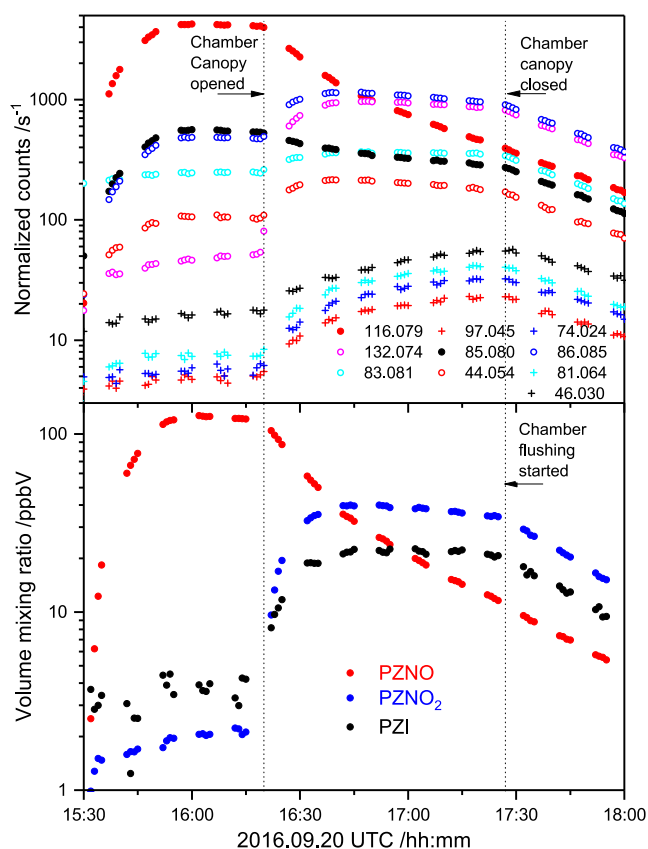


Figure 3. Top: time profiles of ion signals detected during the 1-nitrosopiperazine (PZNO) photolysis experiment on 2016.09.20. Only ion signals increasing by more than 1% of the *m/z* 116.079 [PZNO]H⁺ ion signal decrease are included. Drift tube electric field: *E/N* = 65 Td. Bottom: Derived volume mixing ratios (ppbV) of 1-nitrosopiperazine (PZNO), 1-nitropiperazine (PZNO₂), and 1,2,3,6-tetrahydropyrazine (PZI) during the experiment.

Table 1. Relevant Mass Peaks Detected by PTR–TOF–MS During 1-Nitrosopiperazine (PZNO) Photolysis Experiments

<i>m/z</i>	ion sum formula	interpretation
44.050	C ₂ H ₆ N ⁺	fragment from [PZNO]H ⁺ , [PZNO ₂]H ⁺ and [PZI]H ⁺
83.060	C ₄ H ₇ N ₂ ⁺	H ₂ elimination from [PZI]H ⁺
85.076	C ₄ H ₉ N ₂ ⁺	[PZI]H ⁺ , fragment from [PZNO]H ⁺ and [PZNO ₂]H ⁺
86.084	C ₄ H ₁₀ N ₂ ⁺	fragment from [PZNO]H ⁺ , [PZNO ₂]H ⁺
116.082	C ₄ H ₁₀ N ₃ O ⁺	[PZNO]H ⁺
132.077	C ₄ H ₁₀ N ₃ O ₂ ⁺	[PZNO ₂]H ⁺

that PZNO, PZNO₂, and PZI are neither lost to the chamber 360 walls nor to the aerosol phase in large amounts during the time 361 of photolysis, it is possible to obtain a hypothetical [PZI]H⁺ 362 ion signal using the PZNO and PZNO₂ fragmentations 363 previously determined. The *m/z* 86.084 is fully accounted 364 for by PZNO and PZNO₂, whereas the *m/z* 44.050 (C₂H₆N⁺) 365 also includes the contribution from a ring scission fragment of 366 [PZI]H⁺, and the *m/z* 83.060 (C₄H₇N₂⁺) is explained by H₂- 367 loss from [PZI]H⁺. 368

Figure 3 also includes the derived volume mixing ratios of 369 PZNO, PZNO₂, and PZI. The gas-phase mass balance in the 370 photolysis experiment shown is only around 60%, but more 371

372 than half of the missing mass can be accounted for by OH
373 reactions with PZNO, PZNO₂, and PZI, and partitioning to
374 wall surfaces and to particle formation; see later.

375 Two of the three photolysis experiments were modelled
376 according to Scheme 1 taking the monitor values for NO, NO₂,
377 and j_{NO_2} , and the derived OH-fields as input (the third
378 experiment was carried out under conditions that did not allow
379 quantification of the actinic flux in the chamber). Alike the
380 nitro group, the nitroso group reduces the OH reactivity of
381 (CH₃)₂NNO, ^{37,41} by an order of magnitude vis-à-vis that of
382 the parent amine. ³⁸ The OH rate coefficients for PZNO and
383 PZNO₂, and, for the sake of simplicity, also for PZI were
384 therefore fixed in the model to $1/2 \times k_{\text{OH}+\text{PZ}}$. The rate
385 coefficient for PZNO wall loss was determined to be 4×10^{-5}
386 s⁻¹ from the sample decay prior to opening the chamber
387 canopy; the same value was assumed to apply for PZNO₂ and
388 PZI. Attempts to determine the relative photolysis rate
389 coefficient, $j_{\text{rel}} = j_{\text{PZNO}}/j_{\text{NO}_2}$, from the available data showed a
390 correlation of 0.99 between j_{rel} and k_2/k_4 . Consequently, j_{rel}
391 was constrained to 0.34—the average value reported for other
392 nitrosamines⁸—and only k_2/k_4 and k_3/k_4 were refined in a
393 non-linear least-squared fitting of the experimental data. The
394 derived parameters, $k_2/k_4 = 1.7 \pm 0.3$ and $k_3/k_4 = (1.57 \pm$
395 $0.06) \times 10^{-7}$ (2σ error limits), fall in the range reported from
396 other nitrosamine photolysis studies,⁸ but they should not be
397 compared directly as the chemistry models differ.

398 Figure 4 illustrates the quality of PZNO photolysis modeling
399 under natural sunlight conditions during the afternoon of

walls and to reaction with OH radicals amounts to ~8% each. 409
Finally, we note that there is also a pleasing agreement 410
between the indirectly determined PZI mixing ratios in the 411
photolysis experiments and the modelled PZI mixing ratio, 412
lending confidence to the ion signal interpretation, as 413
presented in Table 1. 414

3.2.4. Piperazine Photo-Oxidation Studies. Previous PZ 415
photo-oxidation experiments carried out in the EUPHORE⁸ 416
and the CSIRO⁹ chambers were severely affected by both wall 417
adsorption/desorption and particle formation. The present 418
series of PZ photo-oxidation experiments was carried out 419
under warmer conditions reducing the wall effects (Table S10 420
in the Supporting Information summarizes the initial 421
conditions in each of the EUPHORE experiments). Figure 5 422

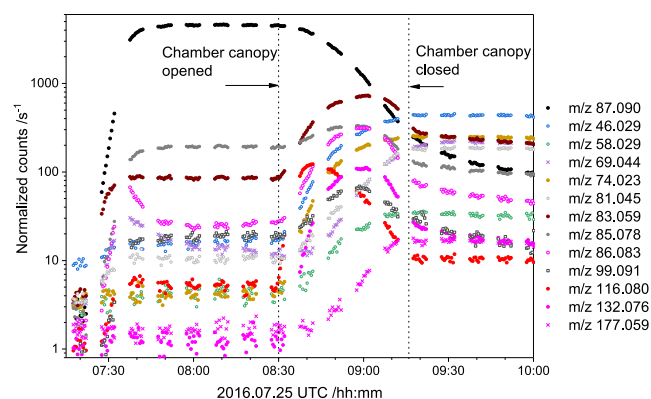


Figure 5. Time evolution of ion signals during the piperazine photo-oxidation experiment on 2016.07.25. With the exception of m/z 177.059 (1,4-dinitropiperazine), ion signals increasing by less than 2% of the piperazine m/z 87.090 signal decrease have been omitted for the sake of clarity. Drift tube electric field $E/N = 105$ Td.

exemplifies the observed time evolution of the major ion 423
signals recorded during a photo-oxidation experiment—for the 424
sake of clarity, only ion signals changing by more than 2% of 425
the change in the piperazine signal m/z 87.092 are included in 426
the Figure. The temporal variation in the NO and NO₂ mixing 427
ratios and in j_{NO_2} are documented in Figure S18 in the 428
Supporting Information. The mass peaks pertinent to the PZ 429
photo-oxidation experiments are summarized in Table 2, which 430
also quotes results from the CSIRO experiments⁹ (Tenax 431
sampling, TD-GCMS); a list of ion signals observed in the new 432
as well as in the previous experiments are collected in Table 433
S11 in the Supporting Information; a cleaned PTR mass 434
spectrum is presented in Figure S19. The availability of data 435
obtained during different years employing different samples 436
and different injection techniques facilitated differentiation 437
between genuine and spurious mass peaks not related to the 438
PZ photo-oxidation per se. (Figure 6) 439

The ion signals can be grouped according to their time 440
evolution: (1) signals that appear upon injection of PZ along 441
with that of m/z 87.090—protonated PZ, (2) signals that grow 442
and decrease again during the photo-oxidation experiment 443
(reactive primary products), and (3) signals that grow steadily 444
after opening the chamber canopy (secondary products and 445
chamber artefacts). 446

The group (1) signals indicate that [PZ]H⁺ fragments at the 447
instrumental conditions are employed in the present experi- 448
ments—although not as severely as protonated PZI, PZNO₂, 449
and PZNO. Analyses of the time periods before photo- 450

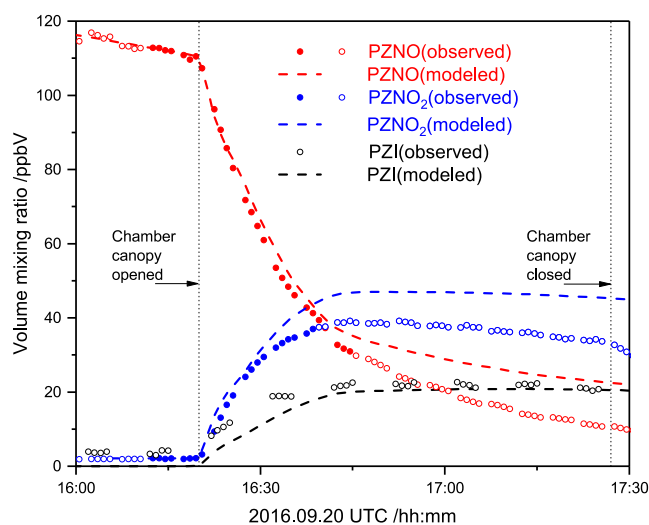


Figure 4. Observed and modelled 1-nitrosopiperazine photolysis under natural sunlight conditions. Observations included in fitting procedure are marked as solid bullets. Abbreviations: PZNO, 1-nitrosopiperazine; PZNO₂, 1-nitropiperazine; PZI, 1,2,3,6-tetrahydropiperazine.

400 2016.09.20 (the other experiment is documented in Figure S16
401 in the Supporting Information). The agreement between the
402 experiment and model is reasonable considering the model
403 constraints, the inherent uncertainties in the monitor values for
404 NO_x and the actinic flux, and the transfer to the aerosol phase,
405 as illustrated in Figure S17 in the Supporting Information.
406 Nearly 10% of the total PZNO/PZNO₂/PZI mass is
407 transferred to the aerosol during the experiment, and the
408 model indicates that total loss of PZNO/PZNO₂/PZI to the

Table 2. Major PTR–TOF–MS Ion Signals Observed During OH Initiated PZ Photo-Oxidation Experiments^a

exact <i>m/z</i>	ion sum formula	fragmentation ^b				interpretation	
		PZ	PZI	PZNO	PZNO ₂		
44.050	C ₂ H ₆ N ⁺	1	12	5	13	ring fragment, aziridine	
46.029	CH ₄ NO ⁺	* ^b				NH ₂ CHO and isomers from heterogeneous reactions, chamber artefact?	
69.045	C ₃ H ₅ N ₂ ⁺	*				imidazole from heterogeneous reactions	
74.024	C ₂ H ₄ NO ₂ ⁺	*				CHONHCHO, primary product	
81.045	C ₄ H ₅ N ₂ ⁺	*	?	?		pyrazine, dehydrogenation fragment from [PZI]H ⁺ and [PZ]H ⁺ ; PZ impurity?	
83.060	C ₄ H ₇ N ₂ ⁺	*	2	84		PZ and PZI dehydrogenation fragment	
85.076	C ₄ H ₉ N ₂ ⁺		3	4	20	30	PZI. fragment of PZ, PZNO, and PZNO ₂
86.084	C ₄ H ₁₀ N ₂ ⁺				12	38	PZNO and PZNO ₂ fragment
87.092	C ₄ H ₁₁ N ₂ ⁺		94				PZ
99.055	C ₄ H ₇ N ₂ O ⁺	*					dihydropyrazinone isomers, oxidation product of PZI?
99.092	C ₅ H ₁₁ N ₂ ⁺	*					unidentified condensation product
115.087	C ₅ H ₁₁ N ₂ O ⁺	*					1-formylpiperazine (cond. prod.)
116.082	C ₄ H ₁₀ N ₃ O ⁺	*			63		PZNO
132.077	C ₄ H ₁₀ N ₃ O ₂ ⁺	*				15	PZNO ₂
177.062	C ₄ H ₉ N ₄ O ₄						PZ(NO ₂) ₂

^aOnly ion signals increasing by more than 2% of the *m/z* 87.092 ion signal decrease are included. Abbreviations: PZ, piperazine; PZI, 1,2,3,6-tetrahydropyrazine; PZNO, 1-nitrosopiperazine; PZNO₂, 1-nitropiperazine. ^bFragmentation in % at *E/N* = 105 Td. Corresponding molecular formula found by TD-GCMS of Tenax samples, ref 9.

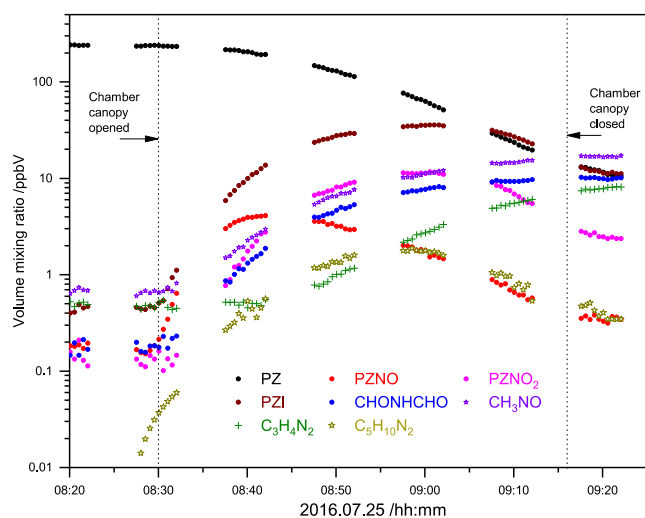


Figure 6. Derived volume mixing ratios (ppbV) of piperazine and observed photo-oxidation products during the experiment on 2016.07.25. Abbreviations: PZ, piperazine; PZNO₂, 1-nitropiperazine, PZNO, 1-nitrosopiperazine; PZI, 1,2,3,6-tetrahydropyrazine; CH₃NO, formamide and isomers; C₃H₄N₂, imidazole and isomers; C₅H₁₀N₂, unidentified condensation product.

oxidation reveals 94% *m/z* 87.092 (protonated molecule), 3% *m/z* 85.076 (C₄H₉N₂⁺, H₂-loss), 2% *m/z* 83.060 (C₄H₇N₂⁺, twofold H₂-loss), and 1% *m/z* 44.050 (C₂H₆N⁺, ring fragment) employing a drift tube *E/N* = 65 Td. In addition, there is an initially correlated mass peak ~0.2% at *m/z* 81.045 (C₄H₇N₂⁺) attributed to protonated pyrazine that may be a sample impurity. Note, however, that *m/z* 81.044 increases in intensity throughout the PZ photo-oxidation experiments, and that it also grows in the PZNO₂ and PZNO experiments.

The group (2) signals include *m/z* 132.077, 116.082, 99.092, 86.084, 85.076, and 83.060. The *m/z* 132.077 is unique to protonated PZNO₂ and is accompanied by fragment ion signals at *m/z* 86.084, 85.076, 57.057, and 44.050; see Section 3.2.2. Likewise, *m/z* 116.0824 is unique to protonated PZNO and is accompanied by fragment ion signals at *m/z*

86.084, 85.076, and 44.050; see Section 3.2.3. The PZNO photo-oxidation experiments established that the present experiments do not singularize a unique mass peak to protonated PZI (*m/z* 85.076), but that *m/z* 83.060 (H₂ ejection from [PZI]H⁺) is characteristic of PZI. Unfortunately, both *m/z* 85.076 and 83.060 also have contributions from [PZ]H⁺ amounting to, respectively, 4 and 2% of the total PZ ion signals. Finally, the *m/z* 99.092 (C₅H₁₁N₂⁺) ion signal originates from an unidentified condensation product.

The group (3) signals include *m/z* 177.062, 99.055, 81.045, 74.024, 69.045, and 46.029. The *m/z* 177.062, unique to PZ(NO₂)₂, shows that the primary products undergo further photo-oxidation during the short timespans of the experiments. The *m/z* 99.055 (C₄H₇N₂O⁺) is tentatively ascribed to dihydropyrazinone—a possible photo-oxidation product of PZI. The *m/z* 81.045 (C₄H₅N₂⁺, protonated pyrazine) signal is puzzling and must have several origins. It clearly correlates with the PZ ion signals before the chamber canopy is opened and with the *m/z* 83.060 PZI ion signal after. However, it increases in intensity until the chamber canopy is closed. The peak at *m/z* 74.023 is assigned to *N*-formylformamide (CHONHCHO), one of the predicted products following H-abstraction from one of the methylene groups in PZ; the yield was estimated on the basis of the calculated dipole moment and isotropic polarizability (Table S1) to be ~4%, which agrees with the high-NO_x predictions of Scheme 1. Alike the PZNO₂ photo-oxidation experiments, ion signals at *m/z* 46.029 (CH₄NO⁺) and 69.045 (C₃H₅N₂⁺) grow throughout the PZ photo-oxidation experiments; the former is assigned to protonated formamide/formamidic acid (CHONH₂/CHOH=NH); the latter is assigned to protonated imidazole.

Figure 7 shows the time evolution of PZ and the photo-oxidation products detected in the gas phase. PZ, PZNO, and PZNO₂ calibration experiments established the yield of PZNO₂ to be 6% after 10 min and 7% after 30 min of reaction in the experiment shown. The maximum amount of PZNO is found to be 9% of reacted PZ after 10 min dropping to 1% after 30 min because of photolysis and decreasing NO content during the experiment. Relying on the *m/z* 83.060

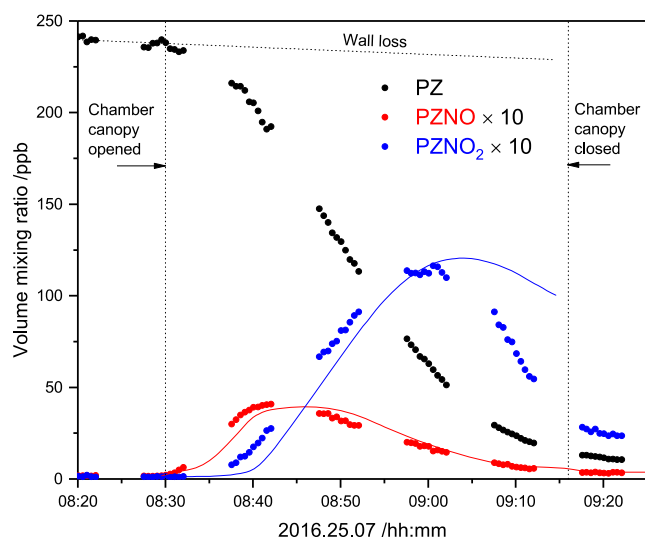


Figure 7. Observed and modeled PZNO₂ formation in the PZ photo-oxidation experiment on 2016.07.25. The full curves represent the model results for $k_{N-H}/(k_{N-H} + k_{C-H}) = 0.20$.

506 intensity and including the intensity-corrected m/z 85.076, the
507 yield of imine was $\sim 30\%$ after 10 min but only $\sim 20\%$ after 30
508 min of reaction.

509 There is a considerable aerosol formation taking place
510 during the experiment, and three of the anticipated products
511 (CHONHCH₂CH₂NHCHO, CHONHCH₂CH₂N=CH₂,
512 and CHONHCH₂OH) that could not be detected in the gas
513 phase with yields $>2\%$ were found in the aerosol, see Section
514 3.2.6. On the other hand, two of the observed gas-phase
515 products (formamide and imidazole), for which there are no
516 obvious gas phase formation routes, can be formed in simple
517 rearrangement reactions of CHONHCH₂OH,
518 CHONHCH₂CH₂NHCHO, and CHONHCH₂CH₂N=CH₂
519 in the aerosol (see Scheme S2).

520 3.2.5. N–H/C–H Branching in the Piperazine + OH
521 Reaction. Onel et al.⁵ studied the PZ + OH gas-phase reaction
522 using the pulsed laser photolysis laser-induced fluorescence
523 technique and reported $k_{N-H}/(k_{N-H} + k_{C-H}) = 0.09 \pm 0.06$
524 from analysis of OH regeneration in the presence of O₂/NO.

525 The present experiments offer an alternative way to obtain
526 the N–H/C–H branching from analysis of the temporal
527 profiles of PZ, PZNO, and PZNO₂ employing the same
528 chemistry model that was used for PZNO photolysis, Section
529 3.2.3, only adding a piperazinyl radical source from the reacting
530 PZ. The model takes NO, NO₂, and j_{NO_2} from the chamber
531 monitors as input. The OH field and the rate coefficient for
532 wall loss are extracted from the temporal PZ profile, and the
533 wall losses of PZNO and PZNO₂ are assumed to be the same
534 as that of PZ. There is a very good agreement between the
535 temporal shape of the OH profiles measured directly by FAGE
536 and those derived from the decay of PZ, although there is a
537 significant difference between the absolute concentrations (for
538 more information, see the Supporting Information).

539 Figure 8 illustrates the results from analysis of the PZ photo-
540 oxidation experiment on 2016.07.25. The PZNO and PZNO₂
541 profiles are reproduced reasonably well with $k_{N-H}/(k_{N-H} +$
542 $k_{C-H}) = 0.2$. Six of the seven new PZ photo-oxidation
543 experiments were carried out under conditions that allowed us
544 to extract an average $k_{1a}/(k_{1a} + k_{1b}) = 0.18 \pm 0.04$ (2 σ

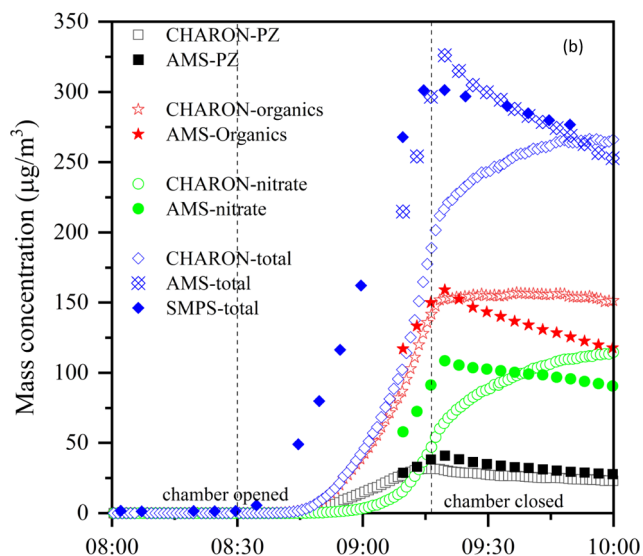
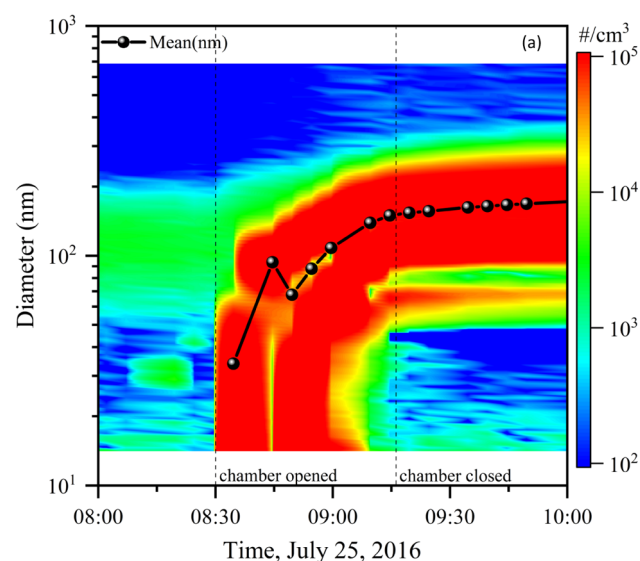


Figure 8. Time evolution of particle size distribution (a) and mass concentrations (b) speciated as PZ, organics, nitrate, and total mass during the PZ photo-oxidation experiment on July 25, 2016.

545 statistical error) that, although notably larger, agrees with the
546 result of Onel et al.⁵ within the combined error estimates.

547 3.2.6. Particle Analysis during the Piperazine + OH
548 Reaction. Figure 8 illustrates the results obtained from
549 analyses of particle data collected during PZ photo-oxidation
550 experiments. The left panel shows how the particle size
551 distribution evolved with time. Particles were already present
552 to sunlight. These particles were formed by the reaction of PZ
553 with HNO₃ (an initial impurity in the NO and later resulting
554 from the NO₂ reaction with OH). Photo-oxidation of PZ was
555 accompanied by strong particle formation, resulting in a total
556 particle mass loading of $\sim 300 \mu\text{g m}^{-3}$ after ~ 45 min of solar
557 radiation. At that time, the particle number concentration was
558 $1.4 \times 10^5 \text{ cm}^{-3}$ and the mean diameter of the particles was
559 approximately 174 nm. Both AMS and CHARON PTR–
560 ToF–MS measurements (right panel) show that a consid-
561 erable part of the total aerosol mass was because of the
562 piperazinium nitrate (note the delay in time response by the
563 CHARON PTR–ToF–MS instrument), but they clearly also 564

565 show that the major fraction of the particle mass was
566 composed of organics other than PZ.

567 **Figure 9** shows the CHARON PTR–ToF–MS mass
568 spectrum collected at 10:00 UTC on 2016.07.25. The most

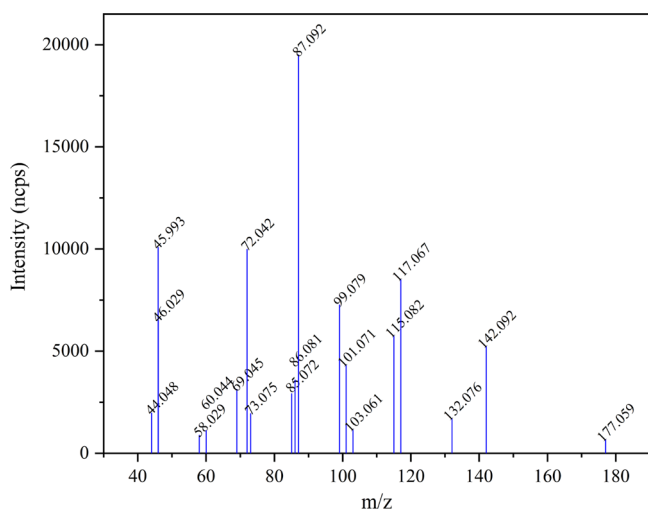


Figure 9. CHARON PTR–ToF–MS mass spectrum obtained from particles formed during 45 min photo-oxidation of a PZ/NO/IPN reaction blend under natural sunlight.

569 abundant peaks at m/z 87.092 ($C_4H_{11}N_2^+$) and m/z 45.993
570 (NO_2^+) are assigned to PZ and nitrate, respectively (nitric acid
571 dehydrates upon protonation in the PTR-MS analyzer).
572 Although most of the aerosol mass peaks observed are also
573 detected in the gas phase (Table 2), there are some important
574 additional ion signals that are assigned to the low volatility
575 products formed upon ring-opening of PZ; see Scheme 1: (1)
576 m/z 58.029 is assigned to $[CHONHCH_2OH]H^+$ dehydrating
577 in the PTR analyzer; (2) m/z 101.071 ($C_4H_9N_2O^+$) is assigned
578 to the protonated imine, $CHONHCH_2CH_2N=CH_2$; (3) m/z
579 117.067 ($C_4H_9N_2O_2^+$) is assigned to the protonated diamide,
580 $CHONHCH_2CH_2NHCHO$. As already addressed in Section
581 3.2.4, these three compounds are expected to undergo simple
582 reactions in the aerosol phase to give formamide/formimidic
583 acid and imidazole.

584 Another important information that can be extracted from
585 the CHARON PTR–ToF–MS mass spectrum is that both the
586 nitramine (PZNO₂, m/z 132.076) and the di-nitramine (di-
587 PZNO₂, m/z 177.059) were observed in the particle phase. In
588 the exemplified experiment, these two species accounted for
589 1.7 and 0.9% of the total aerosol mass, respectively. A strong
590 signature of PZNO₂ was also found in the filter samples
591 analyzed by GC × GC–NCD (see Figure S21 and Table S12
592 in the Supporting Information). PZNO was not detected in the
593 CHARON PTR–ToF–MS mass spectra, while it was found in
594 trace amounts on the filter samples (Table S12). PZI was not
595 detected in CHARON PTR–ToF–MS mass spectra. Imines
596 are highly reactive compounds and are likely to be rapidly lost
597 in the condensed phase.

4. DISCUSSION AND CONCLUSIONS

598 To the best of our knowledge, there are only anthropogenic
599 emissions of PZ to the atmosphere. Once in the atmospheric
600 compartment, PZ will partition between the gas phase and the
601 solid/deliquescent particle phase. Kinetic transfer parameters
602 are needed to describe the partitioning, but no such

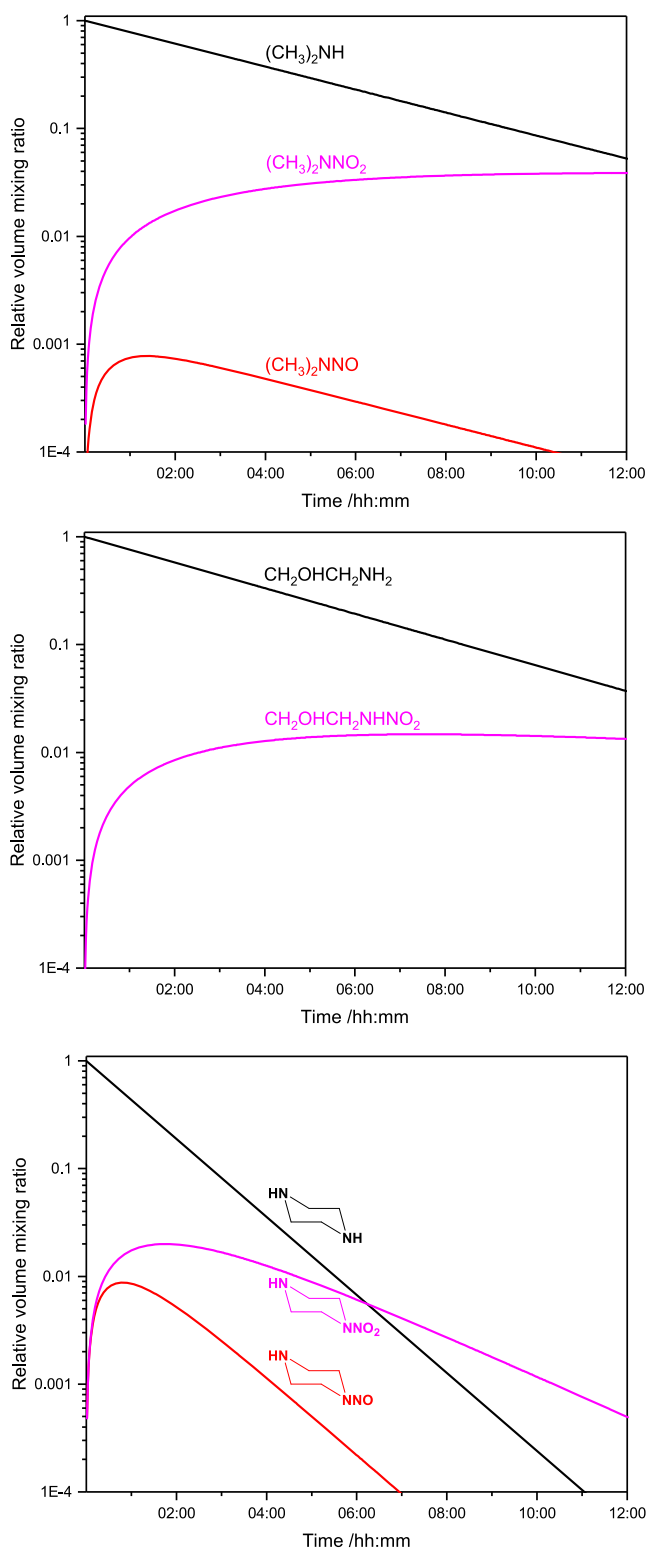


Figure 10. Results from box-modeling the formation of nitrosamines and nitramines in the atmosphere under average conditions in the Oslo region. (top) Dimethylamine, (middle) ethanolamine, and (bottom) piperazine.

603 experimental parameters are available for PZ. Assuming that
604 the measured uptake coefficients for methylamines on S9–82
605 wt % sulfuric acid ($\gamma \sim 2 \times 10^{-2}$)⁴² establish the level to be
606 expected for amine uptake on deliquescent particles in general,
607 the implication is that the aqueous particle uptake of PZ will be

diffusion-controlled under atmospheric conditions. PZ may also form new particles in regions with high levels of acidic compounds. Quantum chemistry calculations of PZ-H₂SO₄ clusters suggest that the homogeneous nucleation process may even compete with PZ removal by OH radicals.⁴³

The Henry's law solubility constant for PZ, determined in thermodynamic calculations, is $H^{\text{CP}} = 1.0 \times 10^2 \text{ mol m}^{-3} \text{ Pa}^{-1}$ (the Henry's law volatility constant $K_{\text{H}} = 1.0 \times 10^{-2} \text{ m}^3 \text{ Pa mol}^{-1} = 9.9 \times 10^{-8} \text{ mol m}^{-3} \text{ atm}^{-1}$).^{44,45} Under nonreactive equilibrium conditions and assuming the liquid water content in clouds, fog, and urban aerosol to be, respectively, 3, 0.2 and $10^{-4} \text{ cm}^3 \text{ m}^{-3}$,⁴⁶ PZ will partition roughly 40, 5, and <1% to the aqueous particle phase in the three cases. Nielsen et al.⁶ have estimated the lifetime of PZ with respect to reaction with OH radicals in typical cloud water and deliquescent particles and reported estimated lifetimes of 1 day in the urban cloud, but just 13 min in the deliquescent urban particles. The high reactivity in the deliquescent aerosol will consequently drive additional uptake to the aerosol, and a non-negligible amount of PZ may actually be oxidized there. It should be noted that there are no experimental results from kinetic and mechanistic studies of aqueous phase piperazine reactions, and only speculations on the possible aqueous phase degradation of piperazine have been reported.⁴⁷

With $k_{\text{OH+PZ}} \approx 2.3 \times 10^{-10} \text{ cm}^3 \text{ molecule}^{-1} \text{ s}^{-1}$, the lifetime of PZ with respect to gas-phase reaction with OH during daytime will typically be around 1 h. The night-time chemistry of PZ is expected to be dominated by the NO₃ radical. However, there is no experimental value for $k_{\text{NO}_3+\text{PZ}}$, but the empirical correlation between OH and NO₃ rate coefficients for reaction with amines implies a very fast reaction, $k_{\text{NO}_3+\text{PZ}} \approx 5 \times 10^{-11} \text{ cm}^3 \text{ molecule}^{-1} \text{ s}^{-1}$ at 298 K.⁶ The average nighttime NO₃ concentration has been suggested to be around $5 \times 10^8 \text{ cm}^{-3}$,^{48,49} which brings the estimated lifetime of PZ during night time to around only a few min. It should be noted that there is no information available in the literature on the branching between N–H and C–H abstraction in amines by NO₃.

The major product in the atmospheric degradation, PZI, is also expected to react quickly with OH and NO₃, but also to enter reversible hydrolysis in aqueous particles introducing additional aldehyde and primary amine functionalities: CHOCH₂NHCH₂CH₂NH₂. Regarding the photo-oxidation products of health concern, PZNO and PZNO₂, the former will primarily undergo very fast photolysis and only a minor fraction will transfer to the aqueous particle phase (the Henry's law solubility constant of the dinitrosopiperazine is virtually the same as that of PZ).⁵⁰ PZNO₂ will undergo relatively fast gas phase photo-oxidation with a few hours' lifetime with respect to reaction with OH radicals with 1-nitroso-4-nitropiperazine and 1,4-dinitropiperazine among the products. There are no data for the Henry's law solubility constants for nitramines, but to a first approximation, they are expected to be the same as those of the nitrosamines. Consequently, the major atmospheric degradation of PZNO₂ is expected to occur in the gas phase.

The present results permit implementation of a consistent PZ gas-phase degradation mechanism in emission dispersion modeling. A simple box model, based on the atmospheric conditions in the Oslo region, suffices to compare the potential health impact of dimethylamine, ethanolamine (MEA), and PZ emissions from a point source (model parameters in Tables

S13, S14). The results, shown in Figure 10, indicate that PZ is the more worrying amine of the three with respect to nitrosamine and nitramine formation per unit of amine emitted. Although the branching between N–H and C–H abstraction in PZ (0.18) is less than half of that of dimethylamine (0.41),⁵¹ the faster PZ reaction with OH, and the slower PZ aminyl radical reaction with O₂, more than counterbalances this. Bearing in mind the dilution of an amine injection with distance from emission point, the calculations show that the maximum potential health impact will arise within the first few km from the emission point.

ASSOCIATED CONTENT

Supporting Information

The Supporting Information is available free of charge at <https://pubs.acs.org/doi/10.1021/acs.jpca.0c10223>.

Details on instrumentation and methodologies including chemical synthesis, atmospheric chemistry of PZ and PZNO₂ from first principles, PZ + OH kinetics study, PZNO₂ photo-oxidation study, PZNO photolysis study, PZ photo-oxidation study, and particle analysis (PDF)

AUTHOR INFORMATION

Corresponding Author

Claus J. Nielsen – Section for Environmental Sciences, Department of Chemistry, University of Oslo, NO-0315 Oslo, Norway; orcid.org/0000-0002-2962-2634; Phone: +47-22855680; Email: c.j.nielsen@kjemi.uio.no

Authors

Wen Tan – Section for Environmental Sciences, Department of Chemistry, University of Oslo, NO-0315 Oslo, Norway
Liang Zhu – Section for Environmental Sciences, Department of Chemistry, University of Oslo, NO-0315 Oslo, Norway
Tomas Mikoviny – Section for Environmental Sciences, Department of Chemistry, University of Oslo, NO-0315 Oslo, Norway
Armin Wisthaler – Section for Environmental Sciences, Department of Chemistry, University of Oslo, NO-0315 Oslo, Norway; orcid.org/0000-0001-5050-3018
Barbara D'Anna – Aix Marseille Univ, CNRS, LCE, UMR 7376, 13331 Marseille, France
Simen Antonsen – Faculty of Chemistry, Biotechnology and Food Science, Norwegian University of Life Sciences, N-1432 Ås, Norway; orcid.org/0000-0002-9416-5476
Yngve Stenstrom – Faculty of Chemistry, Biotechnology and Food Science, Norwegian University of Life Sciences, N-1432 Ås, Norway
Naomi J. Farren – Wolfson Atmospheric Chemistry Laboratories, Department of Chemistry, University of York, York YO10 5DD, U. K.; orcid.org/0000-0002-5668-1648
Jacqueline F. Hamilton – Wolfson Atmospheric Chemistry Laboratories, Department of Chemistry, University of York, York YO10 5DD, U. K.; orcid.org/0000-0003-0975-4311
Graham A. Boustead – School of Chemistry, University of Leeds, Leeds LS2 9JT, U. K.
Alexander D. Brennan – School of Chemistry, University of Leeds, Leeds LS2 9JT, U. K.
Trevor Ingham – School of Chemistry, University of Leeds, Leeds LS2 9JT, U. K.

729 Dwayne E. Heard – School of Chemistry, University of Leeds,
730 Leeds LS2 9JT, U. K.; orcid.org/0000-0002-0357-6238

731 Complete contact information is available at:
732 <https://pubs.acs.org/10.1021/acs.jpca.0c10223>

733 Author Contributions

734 [#]The manuscript was written through contributions of all
735 authors. All authors have given approval to the final version of
736 the manuscript. These authors contributed equally.

737 Notes

738 The authors declare no competing financial interest.

739 ACKNOWLEDGMENTS

740 This work is part of the Atmospheric Chemistry of Amines
741 project (ACA) supported by the CLIMIT program under
742 contract 244055 and has received additional support from the
743 Research Council of Norway through its Centres of Excellence
744 scheme, project number 262695.

745 REFERENCES

- 746 (1) Wilk, A.; Więclaw-Solny, L.; Tatarczuk, A.; Krótki, A.; Spietz, T.;
747 Chwola, T. Solvent Selection for CO₂ Capture from Gases with High
748 Carbon Dioxide Concentration. *Korean J. Chem. Eng.* **2017**, *34*,
749 2275–2283.
- 750 (2) Cousins, A.; Feron, P.; Hayward, J.; Jiang, K.; Zhai, R. *Further*
751 *Assessment of Emerging CO₂ Capture Technologies for the Power Sector*
752 *and Their Potential to Reduce Cost*; CSIRO report EP189975; CSIRO:
753 Australia, 2019.report
- 754 (3) Morken, A. K.; Pedersen, S.; Kleppe, E. R.; Wisthaler, A.;
755 Vernstad, K.; Ullestad, Ø.; Flø, N. E.; Faramarzi, L.; Hamborg, E. S.
756 Degradation and Emission Results of Amine Plant Operations from
757 MEA Testing at the CO₂ Technology Centre Mongstad. *Energy*
758 *Procedia* **2017**, *114*, 1245–1262.
- 759 (4) Låg, M.; Lindeman, B.; Instanes, C.; Brunborg, G.; Schwarze, P.
760 *Health Effects of Amines and Derivatives Associated with CO₂ Capture*;
761 The Norwegian Institute of Public Health, 2011.
- 762 (5) Onel, L.; Dryden, M.; Blitz, M. A.; Seakins, P. W. Atmospheric
763 Oxidation of Piperazine by OH has a Low Potential To Form
764 Carcinogenic Compounds. *Environ. Sci. Technol. Lett.* **2014**, *1*, 367–
765 371.
- 766 (6) Nielsen, C. J.; Herrmann, H.; Weller, C. Atmospheric Chemistry
767 and Environmental Impact of the use of Amines in Carbon Capture
768 and Storage (CCS). *Chem. Soc. Rev.* **2012**, *41*, 6684–6704.
- 769 (7) Lindley, C. R. C.; Calvert, J. G.; Shaw, J. H. Rate Studies of the
770 Reactions of the (CH₃)₂N Radical with O₂, NO, and NO₂. *Chem.*
771 *Phys. Lett.* **1979**, *67*, 57–62.
- 772 (8) Nielsen, C. J.; D'Anna, B.; Bossi, R.; Bunkan, A. J. C.; Dithmer,
773 L.; Glasius, M.; Hallquist, M.; Hansen, A. M. K.; Lutz, A.; Salo, K.,
774 et al. *Atmospheric Degradation of Amines (ADA)*; ISBN 978-82-
775 992954-7-5; University of Oslo: Oslo, 2012, [http://urn.nb.no/](http://urn.nb.no/URN:NBN:no-30510)
776 [URN:NBN:no-30510](http://urn.nb.no/URN:NBN:no-30510); <http://urn.nb.no/URN:NBN:no-30510>.
- 777 (9) White, S.; Angove, D.; Azzi, M.; Tibbett, A.; Campbell, I.;
778 Patterson, M. An experimental investigation into the atmospheric
779 degradation of piperazine. *Atmos. Environ.* **2015**, *108*, 133–139.
- 780 (10) Sarma, P. J.; Gour, N. K.; Bhattacharjee, D.; Mishra, B. K.;
781 Deka, R. C. Hydrogen Atom Abstraction from Piperazine by Hydroxyl
782 Radical: a Theoretical Investigation. *Mol. Phys.* **2017**, *115*, 962–970.
- 783 (11) Ren, Z.; da Silva, G. Atmospheric Oxidation of Piperazine
784 Initiated by OH: A Theoretical Kinetics Investigation. *ACS Earth*
785 *Space Chem.* **2019**, *3*, 2510.
- 786 (12) Ma, F.; Ding, Z.; Elm, J.; Xie, H.-B.; Yu, Q.; Liu, C.; Li, C.; Fu,
787 Z.; Zhang, L.; Chen, J. Atmospheric Oxidation of Piperazine Initiated
788 by Cl: Unexpected High Nitrosamine Yield. *Environ. Sci. Technol.*
789 **2018**, *52*, 9801–9809.
- 790 (13) Tan, W.; Zhu, L.; Mikoviny, T.; Nielsen, C. J.; Wisthaler, A.;
791 Eichler, P.; Muller, M.; D'Anna, B.; Farren, N. J.; Hamilton, J. F.; et al.

Theoretical and Experimental Study on the Reaction of tert-
Butylamine with OH Radicals in the Atmosphere. *J. Phys. Chem. A*
2018, *122*, 4470.

(14) Eichler, P.; Müller, M.; D'Anna, B.; Wisthaler, A. A novel inlet
system for online chemical analysis of semi-volatile submicron
particulate matter. *Atmos. Meas. Tech.* **2015**, *8*, 1353–1360.

(15) Eichler, P.; Müller, M.; Rohmann, C.; Stengel, B.; Orasche, J.;
Zimmermann, R.; Wisthaler, A. Lubricating oil as a major constituent
of ship exhaust particles. *Environ. Sci. Technol. Lett.* **2017**, *4*, 54–58.

(16) Drewnick, F.; Hings, S. S.; DeCarlo, P.; Jayne, J. T.; Gonin, M.;
Fuhrer, K.; Weimer, S.; Jimenez, J. L.; Demerjian, K. L.; Borrmann, S.;
et al. A New Time-of-Flight Aerosol Mass Spectrometer (TOF-
AMS)—Instrument Description and First Field Deployment. *Aerosol*
Sci. Technol. **2005**, *39*, 637–658.

(17) Vaughan, S.; Ingham, T.; Whalley, L. K.; Stone, D.; Evans, M.
J.; Read, K. A.; Lee, J. D.; Moller, S. J.; Carpenter, L. J.; Lewis, A. C.;
et al. Seasonal observations of OH and HO₂ in the remote tropical
marine boundary layer. *Atmos. Chem. Phys.* **2012**, *12*, 2149–2172.

(18) Zhao, Y.; Truhlar, D. G. The M06 Suite of Density Functionals
for Main Group Thermochemistry, Thermochemical Kinetics,
Noncovalent Interactions, Excited States, and Transition Elements:
Two new Functionals and Systematic Testing of four M06-class
Functionals and 12 other Functionals. *Theor. Chem. Acc.* **2008**, *120*,
215–241.

(19) Dunning, T. H., Jr. Gaussian Basis Sets for use in Correlated
Molecular Calculations. I. The Atoms Boron through Neon and
Hydrogen. *J. Chem. Phys.* **1989**, *90*, 1007–1023.

(20) Kendall, R. A.; Dunning, T. H., Jr.; Harrison, R. J. Electron
Affinities of the First-Row Atoms Revisited. Systematic Basis Sets and
Wave Functions. *J. Chem. Phys.* **1992**, *96*, 6796–6806.

(21) Fukui, K. The Path of Chemical Reactions—the IRC Approach.
Acc. Chem. Res. **1981**, *14*, 363–368.

(22) Hratchian, H. P.; Schlegel, H. B. Accurate Reaction Paths using
a Hessian Based Predictor–Corrector Integrator. *J. Chem. Phys.* **2004**,
120, 9918–9924.

(23) Hratchian, H. P.; Schlegel, H. B. *Theory and Applications of*
Computational Chemistry: The First 40 Years; Elsevier: Amsterdam,
2005.

(24) Hratchian, H. P.; Schlegel, H. B. Using Hessian Updating To
Increase the Efficiency of a Hessian Based Predictor–Corrector
Reaction Path Following Method. *J. Chem. Theory Comput.* **2005**, *1*,
61–69.

(25) Adler, T. B.; Knizia, G.; Werner, H.-J. A simple and efficient
CCSD(T)-F12 approximation. *J. Chem. Phys.* **2007**, *127*, 221106.

(26) Knizia, G.; Adler, T. B.; Werner, H.-J. Simplified CCSD(T)-
F12 Methods: Theory and Benchmarks. *J. Chem. Phys.* **2009**, *130*,
054104.

(27) Curtiss, L. A.; Redfern, P. C.; Raghavachari, K. Gaussian-4
Theory. *J. Chem. Phys.* **2007**, *126*, 084108.

(28) Su, T. Parametrization of Kinetic Energy Dependences of Ion–
Polar Molecule Collision Rate Constants by Trajectory Calculations.
J. Chem. Phys. **1994**, *100*, 4703.

(29) Frisch, M. J.; Trucks, G. W.; Schlegel, H. B.; Scuseria, G. E.;
Robb, M. A.; Cheeseman, J. R.; Scalmani, G.; Barone, V.; Mennucci,
B.; Petersson, G. A., et al. *Gaussian 09*, Revision B.01; Gaussian,
Incorporated: Wallingford, CT, 2009.

(30) Werner, H.-J.; Knowles, P. J.; Knizia, G.; Manby, F. R.; Schütz,
M.; Celani, P.; Korona, T.; Lindh, R.; Mitrushenkov, A.; Rauhut, G.,
et al. *Molpro*, version 2012.1, 2012.

(31) Werner, H.-J.; Knowles, P. J.; Knizia, G.; Manby, F. R.; Schütz,
M. *Molpro: a general purpose quantum chemistry program package.*
Wiley Interdiscip. Rev.: Comput. Mol. Sci. **2012**, *2*, 242–253.

(32) Glowacki, D. R.; Liang, C.-H.; Morley, C.; Pilling, M. J.;
Robertson, S. H. MESMER: An Open-Source Master Equation Solver
for Multi-Energy Well Reactions. *J. Phys. Chem. A* **2012**, *116*, 9545–
9560.

(33) Pitts, J. N.; Grosjean, D.; Van Cauwenberghe, K.; Schmid, J. P.;
Fitz, D. R. Photooxidation of Aliphatic Amines under Simulated
Atmospheric Conditions - Formation of Nitrosamines, Nitramines, 860

- 861 Amides, and Photochemical Oxidant. *Environ. Sci. Technol.* **1978**, *12*,
862 946–953.
- 863 (34) Nielsen, C. J.; D’Anna, B.; Karl, M.; Aursnes, M.; Boreave, A.;
864 Bossi, R.; Bunkan, A. J. C.; Glasius, M.; Hansen, A.-M. K.; Hallquist,
865 M., et al. *Summary Report: Photo-oxidation of Methylamine, Dimethyl-*
866 *amine and Trimethylamine. Climit Project No. 201604; NILU OR 2/*
867 *2011*, ISBN 978-82-425-2357-0; NILU, 2011.report
- 868 (35) Atkinson, R.; Baulch, D. L.; Cox, R. A.; Crowley, J. N.;
869 Hampson, R. F.; Hynes, R. G.; Jenkin, M. E.; Rossi, M. J.; Troe, J.
870 Evaluated Kinetic and Photochemical Data for Atmospheric
871 Chemistry: Volume II - Gas Phase Reactions of Organic Species.
872 *Atmos. Chem. Phys.* **2006**, *6*, 3625–4055.
- 873 (36) Maguta, M. M.; Aursnes, M.; Bunkan, A. J. C.; Edelen, K.;
874 Mikoviny, T.; Nielsen, C. J.; Stenström, Y.; Tang, Y.; Wisthaler, A.
875 Atmospheric Fate of Nitramines: An Experimental and Theoretical
876 Study of the OH Reactions with CH₃NHNO₂ and (CH₃)₂NNO₂. *J.*
877 *Phys. Chem. A* **2014**, *118*, 3450–3462.
- 878 (37) Tuazon, E. C.; Carter, W. P. L.; Atkinson, R.; Winer, A. M.;
879 Pitts, J. N. Atmospheric Reactions of N-Nitrosodimethylamine and
880 Dimethylnitramine. *Environ. Sci. Technol.* **1984**, *18*, 49–54.
- 881 (38) McGillen, M. R.; Carter, W. P. L.; Mellouki, A.; Orlando, J. J.;
882 Picquet-Varrault, B.; Wallington, T. J. Database for the Kinetics of the
883 Gas-Phase Atmospheric Reactions of Organic Compounds. *Earth Syst.*
884 *Sci. Data* **2020**, *12*, 1203–1216.
- 885 (39) Geiger, G.; Stafast, H.; Bruehlmann, U.; Huber, J. R.
886 Photodissociation of Dimethylnitrosamine. *Chem. Phys. Lett.* **1981**,
887 *79*, 525–528.
- 888 (40) Peláez, D.; Arenas, J. F.; Otero, J. C.; Soto, J. A Complete
889 Active Space Self-Consistent Field Study of the Photochemistry of
890 Nitrosamine. *J. Chem. Phys.* **2006**, *125*, 164311.
- 891 (41) Zabarnick, S. S.; Fleming, J. W.; Baronavski, A. P.; Lin, M. C.
892 *Reaction Kinetics of Hydroxyl with Nitromethane, Dimethylnitrosamine,*
893 *and 1,3,5-Trioxane; Photolytic Production of Hydroxyl from Nitro-*
894 *methane at 266 nm*; NBS Special Publication: United States, 1986;
895 Vol: 716, pp 731–756.
- 896 (42) Wang, L.; Lal, V.; Khalizov, A. F.; Zhang, R. Heterogeneous
897 Chemistry of Alkylamines with Sulfuric Acid: Implications for
898 Atmospheric Formation of Alkylammonium Sulfates. *Environ. Sci.*
899 *Technol.* **2010**, *44*, 2461–2465.
- 900 (43) Ma, F.; Xie, H.-B.; Elm, J.; Shen, J.; Chen, J.; Vehkamäki, H.
901 Piperazine Enhancing Sulfuric Acid-Based New Particle Formation:
902 Implications for the Atmospheric Fate of Piperazine. **2019**, *Environ.*
903 *Sci. Technol.* - *53*, - 8795. DOI: 10.1021/acs.est.9b02117
- 904 (44) Cabani, S.; Conti, G.; Giannesi, D.; Lepori, L. Thermody-
905 namic Study of Aqueous Dilute Solutions of Organic Compounds.
906 Part 3—Morpholines and Piperazines. *J. Chem. Soc., Faraday Trans. 1*
907 **1975**, *71*, 1154–1160.
- 908 (45) Sander, R. Compilation of Henry’s Law Constants (version 4.0)
909 for Water as Solvent. *Atmos. Chem. Phys.* **2015**, *15*, 4399–4981.
- 910 (46) Herrmann, H. Kinetics of Aqueous Phase Reactions Relevant
911 for Atmospheric Chemistry. *Chem. Rev.* **2003**, *103*, 4691–4716.
- 912 (47) Nielsen, C. J.; Hoffmann, D.; Herrmann, H. *Theoretical*
913 *Evaluation of the Fate of Harmful Compounds Post Emission*; Report
914 2210040-3; Tel-Tek: Porsgrunn, 2010; [https://ccsnorway.com/wp-](https://ccsnorway.com/wp-content/uploads/sites/6/2019/10/atmosphericformation_teltek-2.pdf)
915 [content/uploads/sites/6/2019/10/atmosphericformation_](https://ccsnorway.com/wp-content/uploads/sites/6/2019/10/atmosphericformation_teltek-2.pdf)
916 [teltek-2.](https://ccsnorway.com/wp-content/uploads/sites/6/2019/10/atmosphericformation_teltek-2.pdf)
917 [pdf](https://ccsnorway.com/wp-content/uploads/sites/6/2019/10/atmosphericformation_teltek-2.pdf).
- 917 (48) Atkinson, R. Kinetics and Mechanisms of the Gas-Phase
918 Reactions of the NO₃ Radical with Organic Compounds. *J. Phys.*
919 *Chem. Ref. Data* **1991**, *20*, 459–507.
- 920 (49) Wayne, R. P.; Barnes, I.; Biggs, P.; Burrows, J. P.; Canosa-Mas,
921 C. E.; Hjorth, J.; Le Bras, G.; Moortgat, G. K.; Perner, D.; Poulet, G.;
922 et al. The Nitrate Radical - Physics, Chemistry, and the Atmosphere.
923 *Atmos. Environ., Part A* **1991**, *25*, 1–203.
- 924 (50) Mirvish, S. S.; Issenberg, P.; Sornson, H. C. Air-Water and
925 Ether-Water Distribution of N-Nitroso Compounds - Implications for
926 Laboratory Safety, Analytic Methodology, and Carcinogenicity for Rat
927 Esophagus, Nose, and Liver. *J. Natl. Cancer Inst.* **1976**, *56*, 1125–
928 1129.
- (51) Onel, L.; Blitz, M.; Dryden, M.; Thonger, L.; Seakins, P. 929
Branching Ratios in Reactions of OH Radicals with Methylamine, 930
Dimethylamine, and Ethylamine. *Environ. Sci. Technol.* **2014**, *48*, 931
9935–9942. 932